

Integrating Flexible Filament Circuits for E-Textile Applications

Abiodun Komolafe,* Russel Torah, Yang Wei, Helga Nunes-Matos, Menglong Li, Dorothy Hardy, Tilak Dias, Michael Tudor, and Stephen Beeby

Practical wearable e-textiles must be durable and retain, as far as possible, the textile properties such as drape, feel, lightweight, breathability, and washability that make fabrics suitable for clothing. Early e-textile garments were realized by inserting standard portable electronic devices into bespoke pockets and arranging interconnects and cabling across the garment. In these examples, the textile merely served as a vehicle to house the electronics and had no inherent electronic functionality. A reduction in electronic component size, the development of flexible circuits, and the ability to weave robust interconnects offer the potential for improved levels of electronic integration within the textile. The weaving of electronic circuit filaments less than 2 mm wide into fabrics such that the electronics are fully concealed in the textile and given extra protection by the surrounding textile fibers is introduced. The failure mechanisms for different filament circuit designs before and after integration into the textile are investigated with a 90° cyclical bending test. Results show that encapsulated filament circuits embedded within the textile survive 45 washing cycles and more than 1500 cycles of 90° bending around a bending radius of 10 mm, performing five times better than equivalent filament circuits before integration into the fabric.

1. Introduction

E-textiles (also known as smart fabrics) are textiles that incorporate electronic functionality. E-textile garments enable electronic systems to be mobile, personalized and accessible to

Dr. A. Komolafe, Dr. R. Torah, H. Nunes-Matos,
Dr. M. Tudor, Prof. S. Beeby
Department of Electronics and Computer Science
University of Southampton
Highfield Campus, Southampton SO17 1BJ, UK
E-mail: a.o.komolafe@soton.ac.uk

Dr. Y. Wei
School of Science and Technology
Clifton Campus
Nottingham Trent University
NG11 8NS, UK

Dr. M. Li
School of Materials
The University of Manchester
Sackville Street Building, Manchester, M1 3BB, UK

Dr. D. Hardy, Prof. T. Dias
Advanced Textiles Research Group
School of Art & Design
Nottingham Trent University
Burton Street, NG1 4BU Nottingham, UK

 The ORCID identification number(s) for the author(s) of this article can be found under <https://doi.org/10.1002/admt.201900176>.

DOI: 10.1002/admt.201900176

users anywhere and anytime. E-textiles exploit the universality of textiles which covers all types of woven, nonwoven, and knitted materials/fabrics used in a huge variety of applications from clothing (e.g., fashion, workwear, and protective clothing), interior design (e.g., upholstery and carpets), agriculture (e.g., crop protection), civil engineering (e.g., soil retentions and reinforcement), marine (e.g., sails, inflatables, etc.) and industry (e.g., filters, lifting/conveying, etc.). The functionalization of clothing with electronic intelligence offers benefits in application domains including medical and health-care, fashion, military, first responders, and workwear.^[1,2] In all such applications, it is important that the functional electronics and materials are incorporated in a manner that does not significantly alter the physical properties of the fabric and, unlike previous examples, is invisible to the user. Fabrics are by their very nature highly compliant, soft, and typically

breathable. These properties make fabrics ideally suited for clothing but they make them a very challenging medium on, or in, which electronic functionality must be incorporated.^[3] This is in addition to the reliability/durability challenges presented by the abrasive, compressive, and tensile forces that the fabrics experience during normal use.

The first generation of e-textile garments involved portable conventional electronics being inserted into pockets designed into clothing specifically for that purpose. The LifeShirt from Vivometrics^[4] is an example of a commercialized product from 2001. In these first generation e-textiles, the textile itself played no role in the electronic functionality of the garment and the shirt itself was also heavy, uncomfortable, and unaesthetic. The second generation of e-textile garments include limited electronic functionality added in the form of woven or knitted conductive interconnects,^[5–7] electrodes,^[8,9] and antennas.^[10,11] This generation also demonstrated e-textile prototypes that included sensing functionality such as temperature, heart rate, and gas sensors developed for firefighters within the ProeTEX project.^[12] Commercial second generation products such as the Adidas heart rate monitoring sports bra^[13,14] have also emerged. In all such examples, the electronic processing and wireless communications is performed in a conventional rigid module that snaps onto the garment and must be removed for washing. In the research domain, increased levels of electronic functionality has been demonstrated with minimal compromise on the properties of the fabric by the knitting, weaving,

and embroidering of coated yarns for producing 1D or thread-like electronic devices^[3,15–18] and by the printing of functional materials onto the surface of the textile to realize 2D electronic devices on fabrics.^[19–23] The development of functional thick-film polymer inks has enabled standard high-volume printing techniques that are familiar to the textile industry to be used to integrate a wide range of electronic functionality onto the surface of the fabric.^[19–29] The effect of the printed layers on the feel of the textile and its breathability can be minimized by ensuring the films are flexible, as thin as possible, and only printed where required. Functionality is defined by the ink formulation and includes conductive inks for printed interconnects,^[24] resistive inks for resistors and strain gauges,^[19,25] piezoelectric inks for energy harvesting and sensing,^[26] and electroluminescent inks for displays.^[27] The printing approach is also used to produce electronic circuits, or fabric printed circuit boards (PCBs),^[19,28] on which surface mount electronic components can be bonded using conductive adhesives.^[28,29] However, the durability of these circuits is poor with cracks developing in the conductive inks and conductive adhesives due to mechanical forces and bending. The electronics are also still visible to the wearer and approaches for improving the durability by encapsulation only accentuates the presence of the electronics on the fabric.^[25,30]

The third generation of e-textiles has demonstrated increasing levels of 1D electronic integration within the fabric using flexible plastics as carrier substrates.^[16,31–34] This approach benefits from the use of conventional electronic circuit fabrication techniques on flexible substrates.^[35] The state of the art following this approach is detailed in the work by Cherenack et al.^[33] where periodic weft yarns of a fabric are replaced during weaving with two terminal electronic plastic strips (e-strips) that are interconnected along the warp direction of the fabric with conductive threads. The individual e-strips have been demonstrated with widths between 1 and 5 mm, and incorporating humidity and temperature sensors, thin-film sensors, and LEDs. Mounted electronics and conductive threads are attached using isotropic conductive adhesives and are protected by glob topping. The entire e-strip was encapsulated with a spray-on silicone layer and examples containing a 600 nm thick copper thin film transistors (TFTs) survived 1000 tensile bending cycles around a 10 mm bending radius.^[36,37] Woven textile swatches containing LED e-strips failed after five washing cycles at a 30 °C due to corrosion of the 18 µm thick copper tracks and flaking of the silicone encapsulation on the LEDs.^[32] A further limitation of this embodiment is that the e-strips were still visible to the wearer after integration into the fabric and the effect of the fabric on the reliability of the e-strips have not been investigated. In another form of 1D electronics integration in textiles (e-yarns), Hardy et al.^[38] improved the concealment of electronics into the fabric by integrating two terminal components such as LEDs and thermistors into the core of textile yarns with multistrand copper wires as shown **Figure 1a**. This approach is, however, unsuitable for incorporating complex circuits that typically require multiple connections to circuits and devices. Other forms of 1D electronics are based on using coated textile fibers to realize woven transistor/logic circuits or electrical interconnections on fabrics^[39,40] but like the 2D printed structures, the reliability of

the integrated electronics is largely dependent on the durability of the functional inks that are used to coat the textile fibers and the top layer encapsulation.^[41] In addition to these durability and wearability limitations, the 1D and 2D e-textile prototypes are potential sources of e-waste that may prove ecologically challenging to recycle or dispose if mass produced due to the contamination of the textile host by the functional inks.^[42,43]

This paper addresses the wearability and recyclability of e-textiles using a woven approach that exploits the 1D e-strip concept to achieve flexible modular circuits in the form of filaments and extends the concept by weaving the filaments into the fabric in a manner that conceals its presence from the wearer and uses the surrounding textile fibers/yarns to offer extra protection to the circuits. This approach locates the filament circuits in the body of the fabric during the weaving process by forming bespoke pockets within the structure of the textile as shown in **Figure 1b**. These pockets allow the placement of the filaments and routing of wires within the fabric in a way that has minimal impact on the feel of the fabric and is undetectable by the wearer. It also ensures that the filament circuits can be easily removed and isolated from the fabric to be separately recycled or disposed as electronic waste and thereby preventing any electronic contamination of the fabric. Functioning e-textile swatches implementing components such as LEDs and microcontrollers on demonstrator filaments of widths ranging from 2 mm down to 0.8 mm have been demonstrated. The filament circuits before and after weaving were subject to a cyclical bending and washing routine to investigate the limits of conventional filament circuit design rules and the effect of the bespoke fabric pocket on the electrical and mechanical reliability of the filaments.

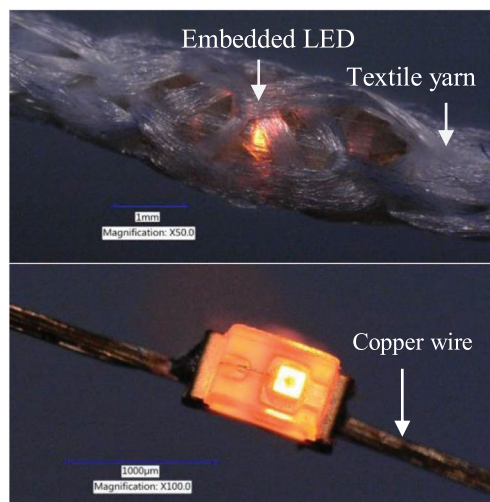
2. Results and Discussions

2.1. Material and Process Selection for Fabricating Filament Circuits

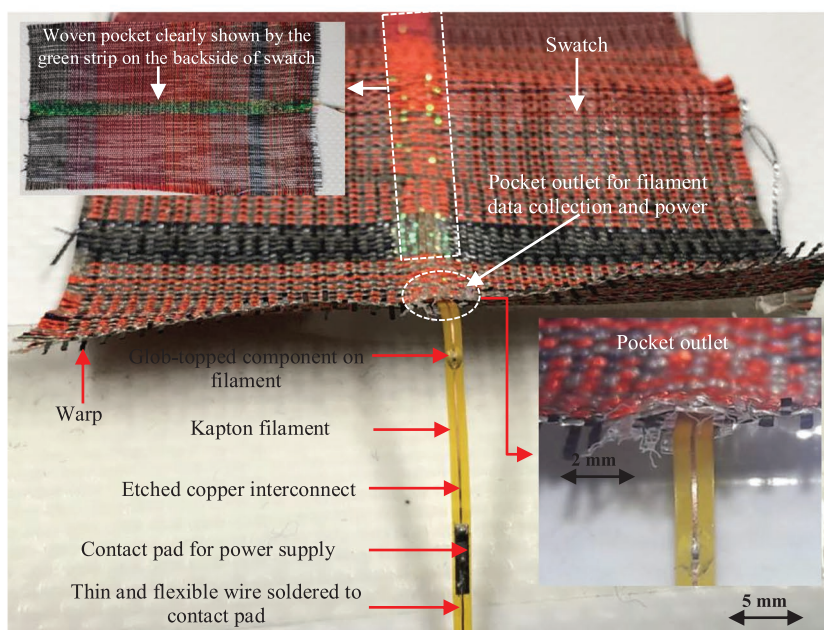
The functional flexible filament circuit shown in **Figure 1b** consists of a substrate, metal interconnections, electronic components, conductive adhesives, or solder pastes for bonding the electronic components and underfill adhesives for improving mechanical strength. Significant research has been undertaken in order to achieve the circuit resolution necessary for integrating bare die components. Different materials, techniques for handling and mounting the components, and design features have been investigated in order to maximize reliability.

2.1.1. Substrate and Adhesive Selection and Characterization

Mechanical reliability is an essential consideration for practical applications of wearable e-textile due to the need to survive bending and washing and this can be influenced by the properties of the substrate material.^[44,45] Components were mounted onto PEEK, Kapton, and Mylar substrates using the different adhesives listed in **Table 1** and were subjected to standard shear and bending tests. The adhesives were found to fail under mechanical loads up to 200 N. The optimum



(a)



(b)

Figure 1. a) An operational LED yarn showing the two-terminal connection of an LED inside a yarn. b) Embedded flexible filament circuit in a textile swatch of a total thickness of 230 μm .

material combination was found to be Masterbond EP37-3FLF with a Kapton substrate. The finite element analysis identified an optimum adhesive thickness between 0.048 and 0.05 mm at which the stress induced within the adhesive due to applied forces is minimized.

2.1.2. Substrate and Adhesive Selection and Characterization

Flexible filament circuits on Kapton were fabricated using three types of metallization: screen printed silver polymer

inks, evaporated thin films (gold and aluminum), and commercially available copper clad Kapton. The screen-printing process is a straightforward method for directly printing the circuit design on the Kapton using flexible conductive polymer inks. However, the bonding of electronic components onto printed inks using standard soldering is not possible due to the high temperatures involved and components can only be attached using conductive adhesives, the mechanical strength of which is inferior to solder. The minimum feature size possible with standard screens is 100 μm , which is suitable for fabricating simple electronic circuits.^[46] As the circuit complexity increases, the required feature size shrinks beyond the limits of standard screen printing. **Figure 2a** below shows an example of printed electronic filament designed to mount 0603 LED packages using isotropic conductive adhesive. The fabricated filaments functioned correctly and survived bending around a 12 mm diameter radius. However, the adhesive was difficult to apply resulting in inconsistent contact resistances and varying illumination intensities. Such adhesives also have a short working time that is not ideal for scaling up to a larger scale commercial process.

Thermal evaporation was used to metalize a 50 μm thick Kapton substrate with 100 nm thick gold and aluminum films. This enables the linewidth and spacing of the circuit to be fabricated down to 1 μm using standard contact lithography and etching. However, several technical issues were encountered. First, the aluminum film exhibited poor adhesion to the Kapton and failed the adhesion tape test. This was solved by oxygen or argon plasma treatment of the surface of the Kapton. Next, suitability for soldering and wire bonding were investigated. Solder bump attachment was found not to be possible due to the gold film burning off during soldering and the incompatibility of the solder with the aluminum. Wedge and ball wire bonding was also not possible because the bond wires would not adhere to either metal films^[47]

even at high bonding forces.^[53] However, when these thin films were replicated on a rigid silicon or alumina substrate, the wire bonding processes worked as expected. This nonstick effect is due to the mechanical properties of the Kapton substrate, which results in the dissipation of the ultrasonic energy during wire bonding. Therefore again electronic components could only be mounted using conductive adhesives. The patterned thin film aluminum filament is shown in **Figure 2b**. Copper clad Kapton from GTS Flexible Materials Ltd. with a copper thickness of 18 μm , adhesive thickness of 17 μm , and Kapton thickness of 25 μm was identified as the preferred solution. The adhesive

Table 1. Material properties of substrates and adhesives.^[44]

Types	Materials	Young's modulus [MPa]	CTE [K ⁻¹]	Density [g cm ⁻³]	Tensile strength [MPa]
Substrates	PEEK	3800	4.7×10^{-5}	1.32	98
	Kapton	2500	2×10^{-5}	1.42	231
	Mylar	3100	1.7×10^{-5}	1.39	138
Adhesives	Dymax 3031	100	178×10^{-6}	1.03	10
	Delo-Monopox NU355	1700	150×10^{-6}	1.1	42
	Delo-Monopox Mk055	3200	6.4×10^{-5}	1.2	50
	EP30A0	3447	25×10^{-6}	1.06	41
	EP37-3FLF	344	9×10^{-5}	1.05	35
	Epo-Tek 301 2fl	3664	56×10^{-6}	1.07	≥13.7
	Loctite 4902	400	425×10^{-6}	1.06	16
	Loctite 4860	430	1×10^{-4}	1.07	≥5
	Loctite 480	2000	8×10^{-5}	1.1	≥1.8

bonding the copper film to the Kapton survives the tape test and the high conductivity and increased thickness of the copper give the lowest track resistance ($\approx 0.003 \Omega \text{ mm}^{-1}$ for a track width of $100 \mu\text{m}$) of the three methods. This compared to track resistances per unit length of the printed $5 \mu\text{m}$ thick silver tracks and 500 nm thick evaporated aluminum are ≈ 0.6 and $82 \Omega \text{ mm}^{-1}$, respectively. The copper film was also fully compatible with soldering and wire-bonding processes enabling a variety of chip mounting and interconnecting processes to be used. Circuit features were fabricated using photolithography and etching (see Figure 2b) and these processes and the minimum feature sizes achievable are discussed in the following section. Kapton

thicknesses from 12 to $125 \mu\text{m}$ and copper film thicknesses ranging from 9 to $105 \mu\text{m}$ are available and bespoke dimensions can be obtained if ordered in large enough quantity.^[48]

2.2. Fabrication of Filament Circuits on Copper-Clad Substrate

The copper clad Kapton substrates were patterned using a wet copper etch and a photoresist masking layer which is discussed in details in the Experimental Section. The minimum feature size is dependent on the thickness of the copper film due to the isotropic nature of the copper etching process that undercuts the

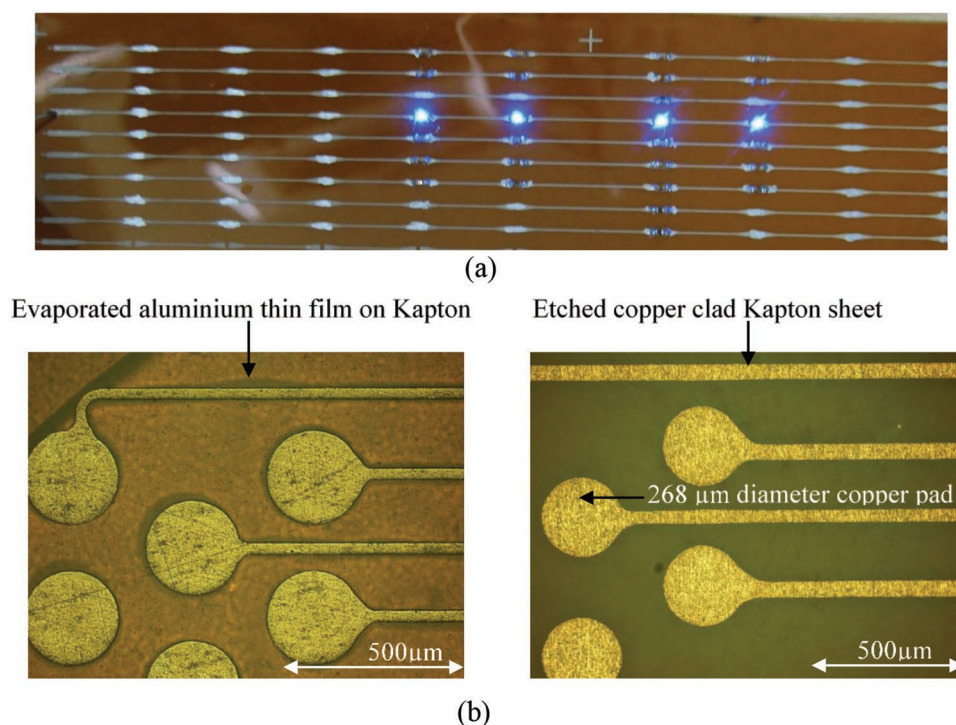


Figure 2. a) Screen printed silver polymer conductors on Kapton with LEDs attached using conductive epoxy and b) filament metallization by thermally evaporated aluminum $30 \mu\text{m}$ wide interconnects (left) and etched copper $55 \mu\text{m}$ wide interconnections (right).

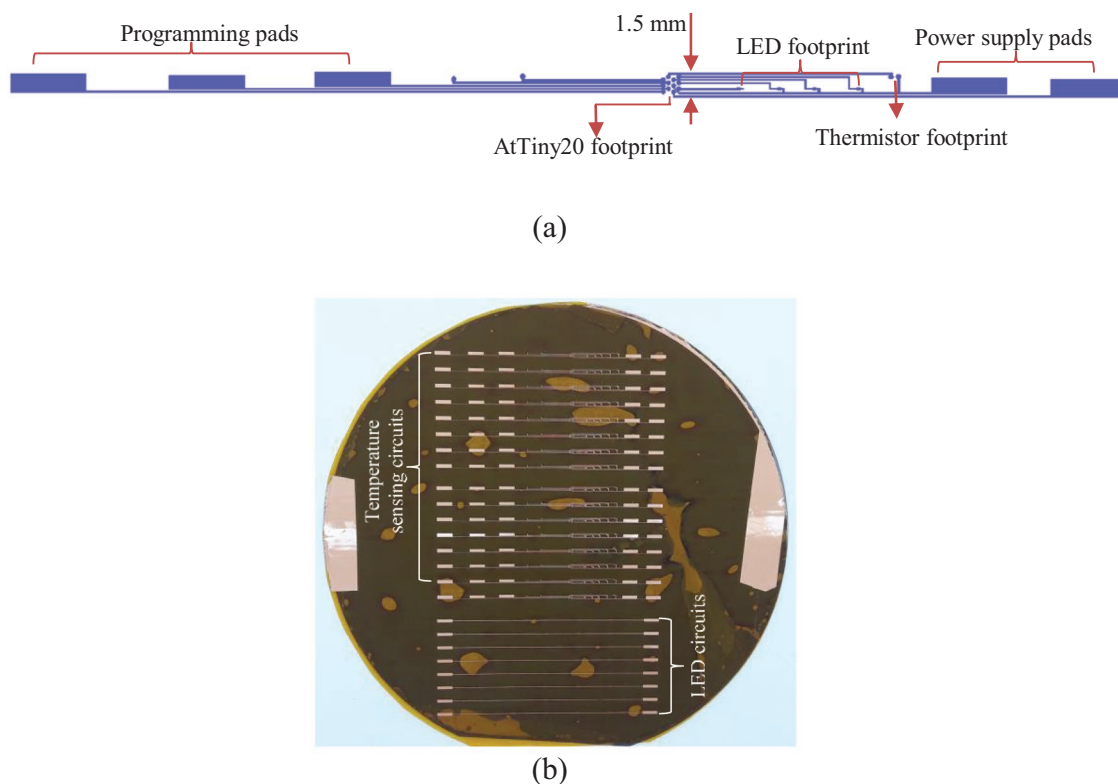


Figure 3. a) Circuit layout of the temperature sensor filament and b) circuit patterns on Kapton sheet after photolithography and etching.

masking layer. For the 18 μm thick copper film, feature sizes of less than 36 μm will result in the mask being completely undercut leaving an uneven copper thickness and inconsistent track resistance. For the 18 μm thick copper film, a sensible minimum feature size is 80 μm and thinner copper films should be used for smaller feature sizes. While the linewidths of circuit should be as fine as possible to minimize the size of the filament, it is important that the track resistivity is low enough to reduce voltage drops across the circuit and, in the case of higher current applications, resistive heating. The IPC-2221 standard for flex circuits for 18 μm thick copper suggests a track width of 24.4 μm for a length of 100 mm and 100 mA current.^[49] The designed circuit is a digitally controlled LED lighting filament containing an Atmel microcontroller, AtTiny20, and LED (as shown in Figure 3a). The addition of a thermistor enables this filament circuit design to also work as a temperature sensor with an LED output. The circuit is 1.5 mm wide and is fitted on a 2 mm wide filament. The copper interconnections are 85 μm wide with a spacing of 96 μm , and a spacing of 25 μm was required between the bond pads of the microcontroller. During fabrication, some air bubbles can be trapped between the copper-coated Kapton and the wafer as shown in Figure 3b, but these were found not to affect the resolution of the fabricated circuits. Using stronger adhesives can reduce these bubbles but this will make the separation of the Kapton sheet from the wafer difficult.

2.2.1. Cutting Patterned Substrates into Strips

Cutting the Kapton into the individual filament strips is not a trivial process and requires a repeatable high resolution process

that produces clean edges. Laser cut tests on uncoated 25 μm thick Kapton were investigated by varying the stage speed, laser power, frequency, and number of passes of the laser. The best results (shown in Figure 4a) were achieved using 30 W laser power, 100% speed, and 5 kHz frequency, producing a 300 μm wide cut.

Although the results are acceptable for a single isolated cut, further testing showed that cutting thin strips (<1 mm wide) from the Kapton was more difficult due to the heat affected zone either side of the cut that would cause the strip to warp. In addition, each cut would produce a significant amount of carbon powder from the burnt Kapton that fouls the surface. Example cuts forming 0.25 mm wide strips are shown in Figure 4b, the warping can be seen where the right hand sections of the strip have raised up from the surface, affecting the width of subsequent cuts. An alternative approach was investigated using an automated flatbed cutter/plotter. The best results on Kapton are shown in Figure 4c and were achieved using a cutting speed of 300 mm s^{-1} and a force setting of 14. The cutter can provide accurate cutting and a smooth, clean edge to the strip with no warping or fouling caused when cuts are in close proximity unlike the laser cutter.

2.2.2. Attachment of Components

Two different types of pastes, anisotropic conductive paste (ACP) and solder paste were investigated for attaching components on the filaments using a Fineplacer lambda commercial pick and place tool as shown in Figure 5. The tool is designed to handle components of minimum dimensions of

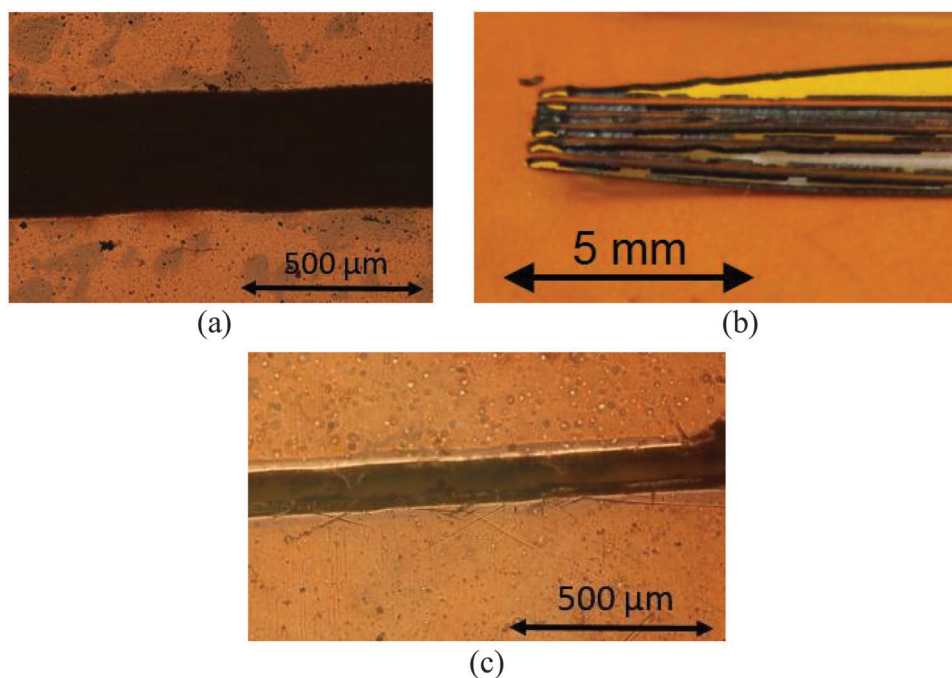


Figure 4. a) Example laser cut with best settings, 50% power, 100% speed, producing a 300 μm wide cut. b) Example of warping and excess carbon fouling from 0.25 mm laser cuts in Kapton and c) example Graphtec cut at 300 mm s⁻¹ with a force setting of 14, producing a 100 μm wide cut.

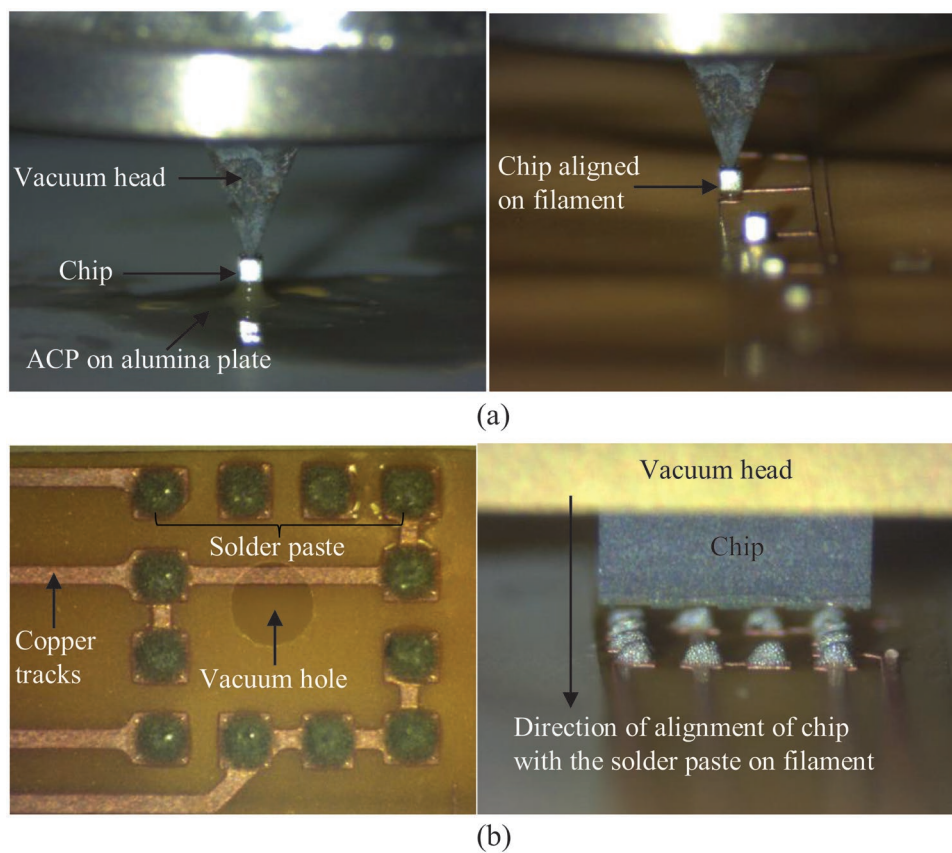


Figure 5. a) Mounting of a thermistor chip with ACP and b) mounting of components on filament using stencil printed solder paste.

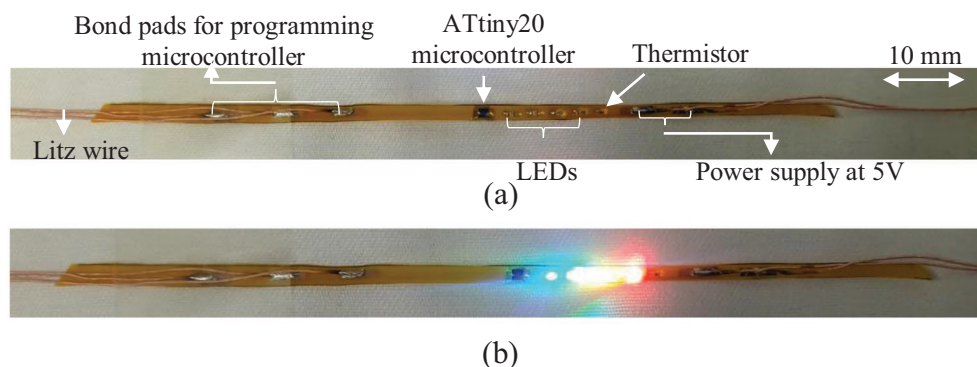


Figure 6. a) Mounted components on a filament using soldering and b) an operational digitally controlled LED filament switched on at 5 V.

0.1 mm × 0.1 mm × 0.1 mm. The use of the tool for the different pastes is discussed in detail in the Experimental Section.

Anisotropic Conductive Pastes: ACPs are ideal for attaching components on circuits with very small (<60 μm) pitch and spacing between footprints. This is because they provide electrical conduction in the vertical direction and prevent short circuits between interconnections that are in close proximity. They also act as an underfill for the components thereby improving the bond strength to the substrate. Sixteen LED filament circuits were produced using the ACP. The mechanical attachment was successful but components were found to be electrically unreliable when the filament was flexed or bent. The contact resistance of the electrical connection varies with strain.

Solder Pastes: Initially, solder paste (BLT Circuit Services type 4 lead free) was pneumatically dispensed on the filament on each bond pad. However, the small volume of paste (picoliters) required a nozzle diameter <150 μm which was found to get clogged by the conductive particles in the pastes. Therefore, the solder paste was printed using a 100 μm thick stainless steel stencil aligned with the substrate producing solder bumps on the surface as shown in Figure 5b. Solder plus underfill was found to provide a mechanically and electrically reliable bond and the connection wires to the circuits were also soldered as shown in Figure 6.

2.3. Weaving Filament into Fabrics

The weaving process for the filaments into fabrics using a commercial dobby weaving loom is discussed in details in the Experiment Section. The fabricated demonstrators include a digitally controlled LED or temperature sensing filament and passive LED filament circuits as shown in Figure 7. The LEDs on the temperature sensing filament light up in turn with increasing temperature. The temperature thresholds are defined in the microcontroller and are fully adjustable. The filament has been designed to respond to body heat and could form a visual digital thermometer, with blue light signaling “cold (<10 °C)” and the red light signaling “hot (>40 °C)” conditions (Figure 7a). Alternatively, the LEDs are driven directly from the microcontroller enabling, for example, a random pattern (Figure 7a). These filament circuits are reprogrammable after integration and can be adapted to suit desired applications.

Figure 7b shows LED filaments woven into a textile swatch. The power supply wires coming out from the woven pockets were laced back through the edge of the swatch and stitched in place before connecting to a coin-cell holder fastened to the backside of the swatch. A 3 V coin-cell powers the swatch and, in contrast to previous works,^[31–33] the filaments are completely concealed in the textile swatch and the LED is only visible when turned on.

2.4. Bending Test

The minimum filament width (*W*) for a circuit containing the smallest available microcontroller (ATtiny20) is 2 mm. The

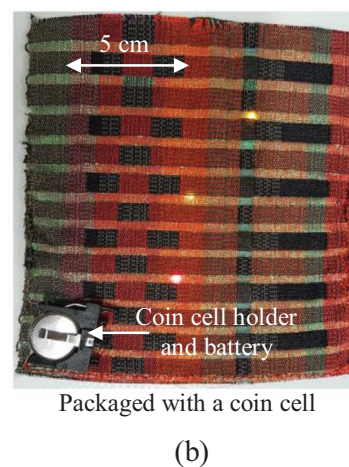
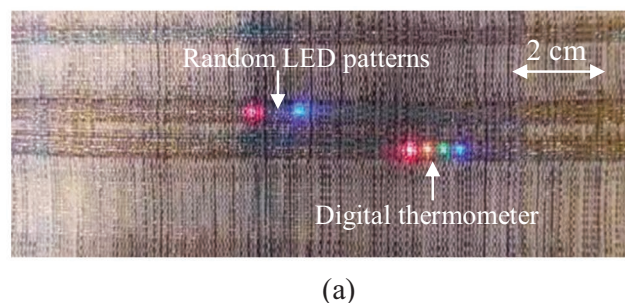


Figure 7. a) Woven fabric containing digitally controlled LED filaments with random patterns and a digital thermometer. b) Woven fabric swatch containing passive LED filaments with a 3 V coin-cell integration.

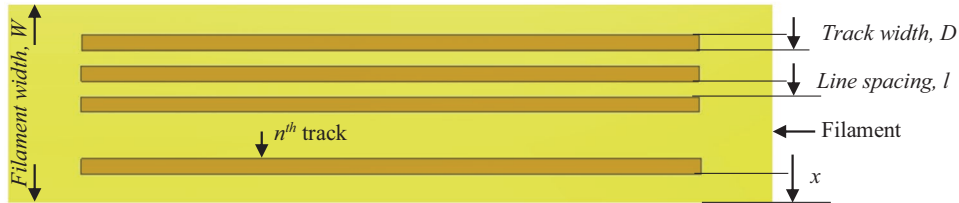


Figure 8. Positioning conductive tracks on filament of width, W .

number of electrical interconnections (or conductive tracks), n , that can be positioned symmetrically on the filament can be calculated from Equation (1), where l is the line-spacing between

the tracks, x is the distance between the outer most tracks and the edge of the filament, and D is the track width as shown in **Figure 8**

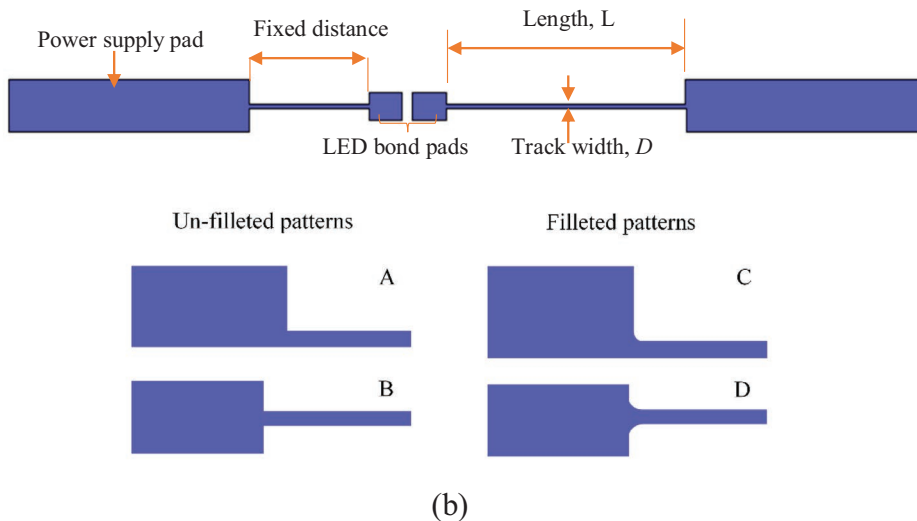
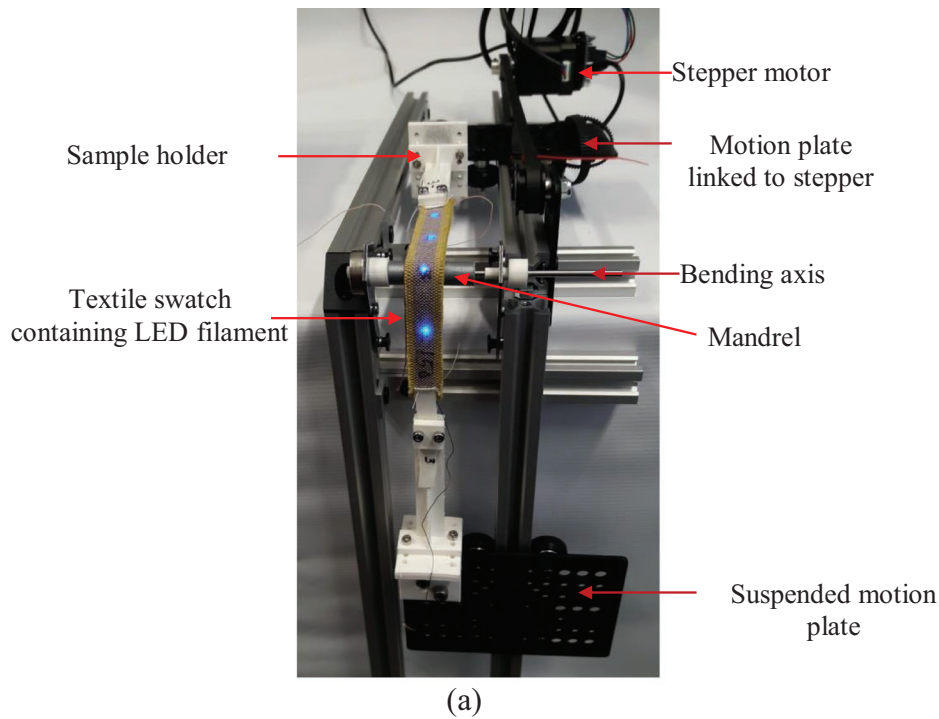


Figure 9. a) Filament circuits with swatch sample shown under 90° bending test. b) Circuit designs for filament showing filleted and unfilleted patterns at bond pad/track joint.

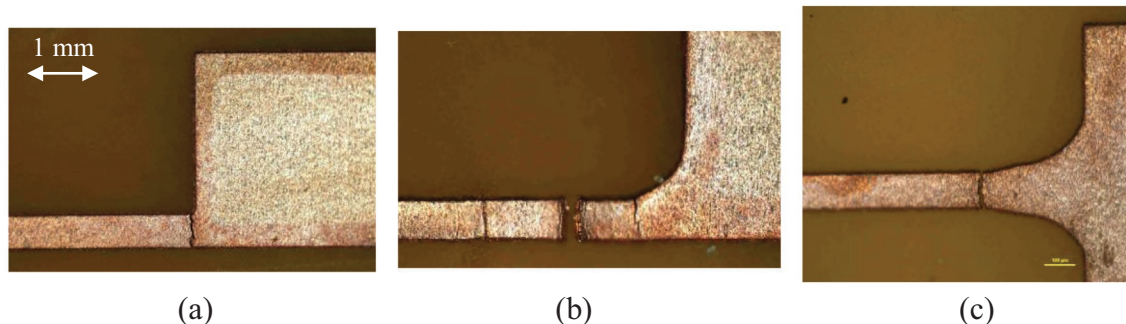


Figure 10. Postbending failure points on 150 μm wide copper tracks a) with no fillet to the bond pads, b) filleted at the edge of the bond pad, and c) filleted at the center of the bond pads.

$$n = \frac{W + l - 2x}{l + D} \quad (1)$$

As the value of “ n ” increases, the track width D must reduce in order to maintain the 2 mm circuit width. In general, circuits with $D \geq 200 \mu\text{m}$ give good performance^[35] and based on Equation (1) this will enable circuits with $n \leq 5$, when $l = 200 \mu\text{m}$ and $x = 100 \mu\text{m}$. The gap sizes between bond pads on the ATtiny20 require the value of D to be less than 200 μm .

The influence of track width and length on circuit reliability was explored from the 90° bending test shown in Figure 9a performed on the LED filament circuits in Figure 7c for track widths, $D = 80, 100, 150,$ and 200 μm and track length, $L = 2.5, 5, 7.5,$ and 10 mm. Track widths will reduce by 36 μm after etching due to undercut of the copper. To investigate failure at the joint between the tracks and the bond pads, different joint designs^[35] were tested as shown in Figure 9b.

2.4.1. Effect of Bending on Filleted and Unfilleted Bond Pads

Examination of filaments after bending indicated the joint between the track and bond pad is a failure point (Figure 10a) and showed that the addition of the fillets in the design affects the location of the break (see Figure 10b,c) but do not prevent these from occurring. The filleted filaments did not perform any better than the unfilleted filaments because the average number of bending cycles in both cases before failure was 62 cycles for a track width of 150 μm .

2.4.2. Effect of Bending on Filaments with and Without Glob-Top Encapsulation

The LEDs on nine bare filaments were glob-topped using UV-curable polymer EC-9519 and the results were compared with seven unencapsulated bare LED strips. The glob top was nozzle dispensed at a pressure of 22 kPa and UV cured for 30 s. Samples were tested around a 5 mm bending radius and the results are shown in Figure 11. The glob-topped filaments survive on average twice the number of cycles of the unencapsulated samples. The filaments without glob top failed due to the presence of

cracks at the point where the copper tracks terminate on the LED bond pad as shown previously in Figure 10 and with the LED in place in Figure 12. For the glob-topped filaments, the failure point is moved to the interface where the glob top terminates on the copper track as shown in Figure 12. The glob top protects the circuit around the LED making the circuit stiffer in this region and delays the onset of the cracking in the copper track.

2.4.3. Effect of Track Width, Bending Radius, and Fabric Swatch

The bending results in Figure 13 show that the average number of cycles survived by the filaments increases with increasing track width and bending radius. Samples with track width of 80 μm performed particularly poorly and almost 50% of the test samples failed before testing due to handling. Hence these samples were not integrated into the swatch. The fabric swatch doubles the average cycles survived by the glob-topped filaments for all track widths at a bending radius of 5 mm. In the swatch samples, the fabric is clamped directly and the tension is acting along the fabric instead of being directly applied to the filaments. Fabric samples with $D = 200 \mu\text{m}$ filaments survived 1500 cycles at a tension of 0.5 N and a bending radius of 10 mm.

The failure modes shown in Figure 14 apply to all filaments both integrated in the textile and freestanding across all bending radii. The failure modes include breaks in the copper tracks, the development of cracks on the glob-top encapsulation,

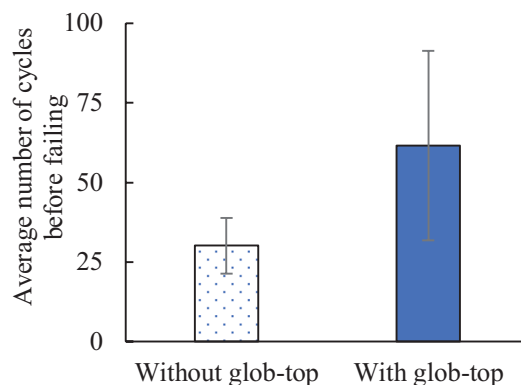


Figure 11. Impact of glob topping on durability of filament circuit.

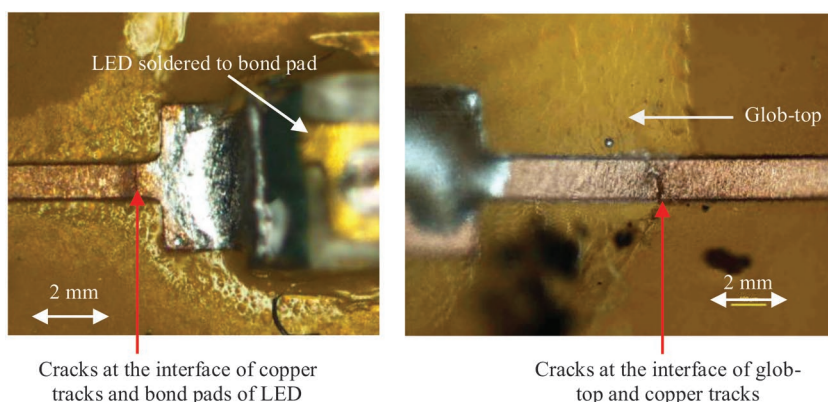


Figure 12. Postbending failure modes on 150 μm wide copper tracks on filament with (right) and without (left) glob-top encapsulation.

and flaking and buckling of the copper tracks due to adhesion failure between the copper and the Kapton filament. The flaking of the copper tracks were common for filaments with track width $D = 80 \mu\text{m}$.

2.4.4. Maximum Cyclic Strain Range, $\Delta\varepsilon_{\text{max}}$, Induced on Filaments in Bending

Three bending radii, $r = 1.5, 5, \text{ and } 10 \text{ mm}$ were used in the bending test. The deformation of the filament circuit (without the fabric swatch) as it bends around the mandrel is shown in **Figure 15**. The neutral axis (NA) positions (where the strain $\varepsilon = 0$) of the filament before and after integration into the fabric are 48.5 and 296 μm , respectively. These were calculated from Equation (2)^[30,50] based on the material properties listed in **Table 2**. In both cases, the elastic modulus of the copper dominates the composite structure such that the NA positions are located within the copper layer close to the boundary between copper and adhesive films. Given these NA values, the induced

strain at any point “ y ” from the center of the filament is obtained from Equation (3)^[30] and the maximum strain range $\Delta\varepsilon_{\text{max}}$ is the sum of the compressive and tensile strains. As expected, the $\Delta\varepsilon_{\text{max}}$ results given in **Table 2** show that the strain induced on the filaments reduce as the bending radius is increased. For filaments within the swatch, the fabric reduces the strain induced on the copper by 26% (i.e., a strain difference of 0.0012) for $r = 5 \text{ mm}$. This explains the increased fatigue lifetime (i.e., number of cycles before failure) of the filaments in the swatch samples as shown in **Figure 13**. However, the strain results and the NA representation in **Figure 15** still indicate the need to reduce the thickness of the copper so that the film is

located closer to the NA thereby enhancing its fatigue life

$$NA = \frac{\sum_{i=1}^n E_i t_i \left(2 \sum_{j=1}^i t_j - t_i \right)}{2 \sum_{i=1}^n E_i t_i} \quad (2)$$

$$\varepsilon = \frac{y - \delta}{\rho} \quad (3)$$

where “ n ,” E_i , and t_i in Equation (2) are the total number of layers, elastic modulus, and thickness of the “ i th” layers in the filament, respectively.

2.5. Effect of Washing on Filaments Integrated within the Fabric

Five glob-topped filaments in two swatch samples as shown in **Figure 7b** were subjected to the ISO 6330:2000-6A washing standard as described in Section 4. Filaments of $D = 200 \mu\text{m}$ were used for the wash test since they performed best in bending. After five washing cycles, interfacial cracks surfaced between the copper tracks and the power supply bond pads on the filaments as shown in **Figure 16**. Dendritic stress marks had also grown on the polyimide base in the region where the copper track interfaced the bond pad as shown in **Figure 16b**. These stress dendrites were not visible in other areas on the filament which suggests that the copper track-bond pad interfaces constitute a major failure/stress point for the circuits and the polyimide substrate. The glob-top encapsulations were unaffected by the washing and all samples worked when probed before the interfacial cracks. Further testing with a different encapsulation method that completely protects the copper tracks and the chip using a thermally molded polyimide filament^[52] increased the washing span of the filaments to 45 cycles.

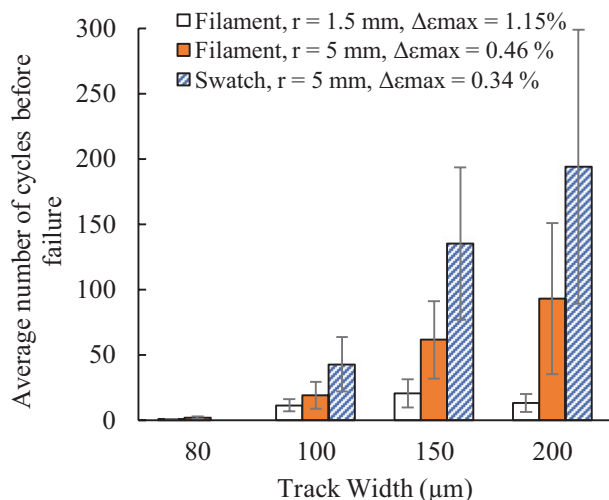


Figure 13. Effect of fabric swatch on the reliability of filament circuit, r is the bending radius and $\Delta\varepsilon_{\text{max}}$ is the maximum strain on the copper film.

2.6. Challenges for Integrating Filament Circuits in Textiles

There are a significant number of challenges to overcome in fabricating flexible filament circuits suitable for integration

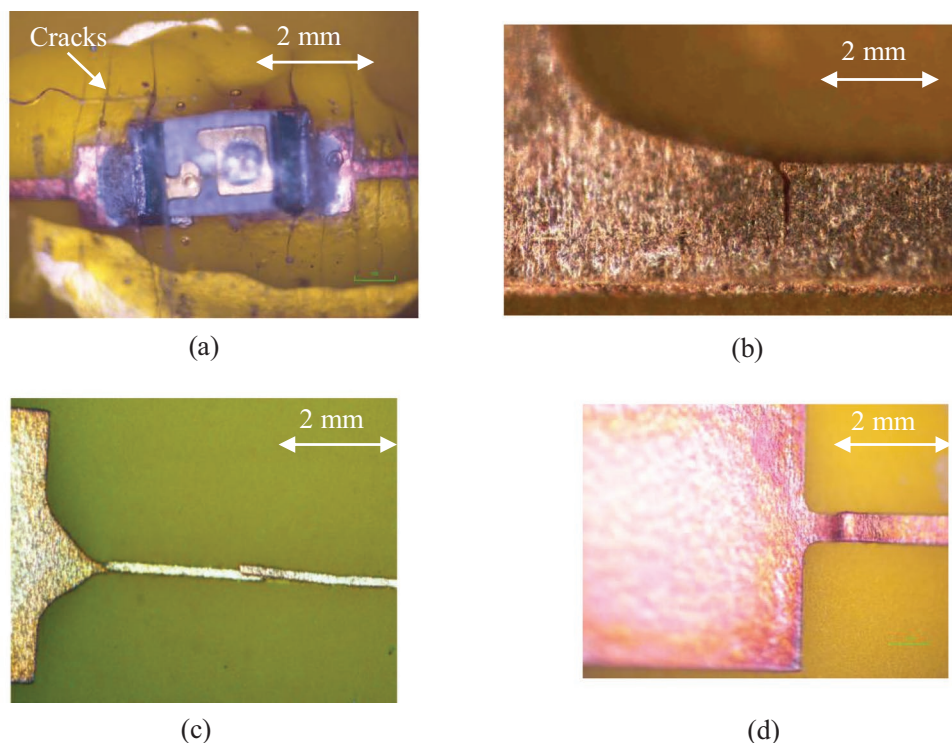


Figure 14. Postbending failure modes of circuits. a) Cracks forming on glob-top encapsulation at 1.5 mm bending radius, b) microfractures forming on 150 μm wide copper tracks close to the bond pads, c) flaking of 80 μm copper tracks due to adhesion failure, and d) buckling of 150 μm wide copper track due to adhesion failure.

inside yarns or woven into the textile. Wherever possible, scalable processes have been used to enable future mass manufacture, which is essential for achieving low cost solutions.

2.6.1. Cutting Filament Circuits for E-Textiles

The goal of this technology is to ultimately produce filaments of <0.5 mm width and reliably cutting filaments that are up

to 15 cm long and 0.5 mm wide is not trivial. The automated scalpel cutter has proved to be capable of meeting this requirement and produced smooth, repeatable cuts with no additional damage to the substrate. Furthermore, larger roll-to-roll cutters of this type are commercially available thus making this a viable approach for mass production. The lab-based cutter used in this work is not able to cut the filaments after the components have been mounted which complicates subsequent assembly and this would have to be addressed.

2.6.2. Mounting Components on Filaments

Mounting the components to the filament circuits is also not straightforward. Bond pad sizes of less than $300 \mu\text{m}^2$ present a challenge when dispensing solder pastes, but stencil printing is suitable and is a process widely used in the printed circuit board industry. The stencils used for larger components (e.g., 0805 package) are 100 μm thick and this results in a paste transfer efficiency (TE) higher than 0.66, which is the minimum surface area ratio (SAR) necessary to achieve a complete paste transfer from the stencil to substrate (IPC-7525 standard). However, as the size of the component and pitch is reduced, as is the case in this research, achieving a surface area ratio in excess of 0.66 becomes challenging because the stencil thickness must be reduced accordingly. This complicates the stencil manufacturing process and increases the difficulty of handling the stencil during use. The minimum feature in this work is $60 \mu\text{m} \times 170 \mu\text{m}$, and the resulting SAR from a 50 μm thick

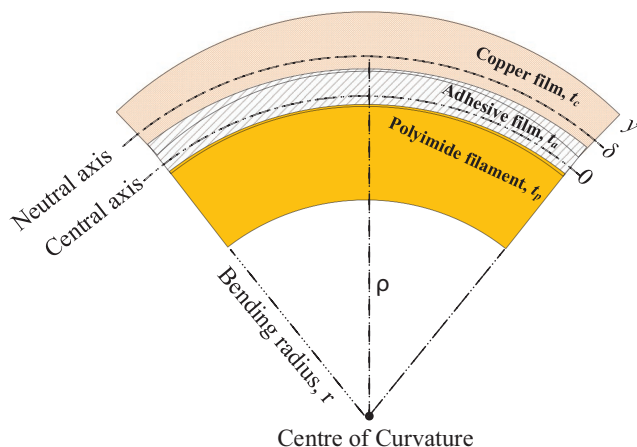


Figure 15. The bending of a filament circuit around a mandrel of radius, r , where ρ and δ represent the distance of the NA from the center of curvature and central axis, respectively.

Table 2. Material properties of filament circuit.

Materials	Thickness, t [μm]	Elastic modulus, E [GPa]	NA position [μm]		$\Delta\epsilon_{\text{max}}$ without swatch [%]		$\Delta\epsilon_{\text{max}}$ with swatch [%]	
			Without swatch	With swatch	$r = 1.5$ mm	$r = 5$ mm	$r = 5$ mm	$r = 10$ mm
Copper	18	70 ^[51]	48.5	296	1.15	0.46	0.34	0.18
Adhesive	17	1.8			1.94	0.58	0.51	0.28
Apical polyimide	25	3			4.6	1.43	1.3	0.69
Swatch	496	0.155			–	–	11.63	5.99

stencil is 0.44 which is below the minimum IPC-7525 standard. In addition to the stencil, the type of solder paste is also critical. Solder paste consists of liquid flux and alloy particles. The alloys used in the solder paste are typically soft metals that are easily deformed while printing. A typical rule of thumb within the PCB industry is that the solder particle should be five times smaller than the minimum stencil aperture width. Commercial type 3 (particles size between 25 and 45 μm) and type 4 (20–38 μm) pastes are often used but, for smaller components (<100 μm), type 5 (15–25 μm) or even type 6 (15–25 μm) may be needed to achieve an optimized paste transfer in conjunction with a thin stencil. The type 4 solder paste used in this work for mounting the electronic components has a maximum particle size half that of the minimum feature size on the stencil. This introduces the difficulty of applying sufficient alloy particles on to the filament circuit, thereby reducing the yield of the soldering process. This challenge will be addressed by evaluating the other types of paste with a smaller particle size.

2.6.3. Durability of Woven Filaments in Fabrics

At present, filament circuits are manually inserted in the pockets during weaving and the placement accuracy can be challenging because of the surrounding fabric yarns. Automating this process will allow high throughput for the mass production. It would improve the placement accuracy of the filaments within the fabric and prevent poor handling of the filaments before they are embedded. The durability of the embedded filament circuits in the textile is also crucial. Embedded filament circuits must be reliable over the lifetime of the fabric to be useful in many applications. With

glob-top encapsulations, these filaments can survive more than 1500 bending cycles at a 1 cm bending radius. However, the bending and washing results show that the durability achievable with glob-top encapsulation of components is limited by the migration of stress points to other areas on the filament circuit that are not protected. To eliminate the stress points, the entire filament should be uniformly encapsulated. This can be achieved by sealing the filament circuit with another layer of Kapton or a thermoplastic material such that the circuit is located at the neutral axis.^[52,53] Although with the use molded Kapton, filaments survive 45 wash cycles but there is need for new methods to optimize the filament circuit design so that interconnect lines are reliably terminated on the larger bond pads where external circuitry or power sources are connected. These approaches will improve the lifetime of integrated filaments in fabrics under bending and washing stresses which are typical stresses for fabrics.

3. Conclusion

This paper described a technology that allows electronic circuits to be fully concealed and integrated within a fabric. Prototype fabrics have been demonstrated that contain 2 mm wide filament circuits successfully incorporated inside bespoke pockets during the garment manufacture. The filament circuits contain sensors and processing capabilities and represent the state of the art in terms of e-textile functionality and integration. This is particularly promising for healthcare applications where electronics for remote monitoring of patients can remain invisible and nonintrusive to the patients leading to improved user acceptability and compliance.

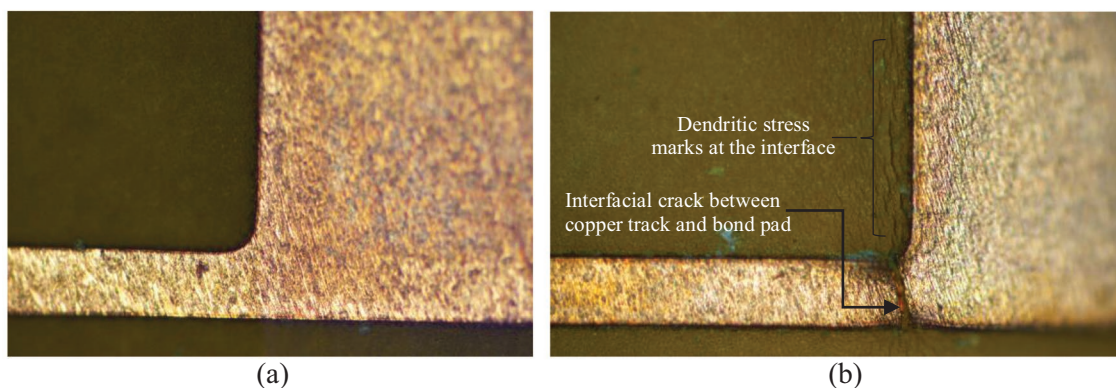


Figure 16. A comparison of filament circuits a) before and b) after washing showing interfacial cracks and dendritic stress mark growth.

Table 3. Temperature profile for soldering of chip.

Process step	Temperature [°C]	Duration [s]
Ramp up rate	$T < 150$	10
Preheat soldering temperature	150	25
Second ramp up rate	150–240	10
Peak temperature	240	10
Ramp down	$T = 40$	15

Currently, the integrated circuits on the filaments are etched from 18 μm thick copper material but the reliability of the filament circuits degrade significantly during bending as the track width of circuit reduces beyond 200 μm . As the copper thickness reduces, the integrated electronics can be easily positioned in close proximity to the neutral axis with new encapsulation methods and materials that would improve the fatigue life of the filaments after integration. The interfacial cracks between the copper tracks and the bond pads for connecting to external circuitry are also a major failure mode limiting the bending and washing of the filaments. Methods for optimizing filament circuit design, to achieve reliable

interfaces between interconnects and bond pads (or encapsulation materials) are still needed to significantly reduce interfacial failures.

4. Experimental Section

Fabrication of Filament Circuits on Copper-Clad Substrate: The copper-coated Kapton was mounted on a 150 mm diameter silicon handle wafer using a wet resist bonding layer and was patterned using contact based photolithography process. A 6 μm thick film of AZ9260 positive photoresist was deposited (spin speed of 3000 rpm for 30 s and oven baked for 3 min at 110 °C) and patterned using an EVG 620T contact mask aligner with a 20 s exposure at an energy density of 8.88 mW cm^{-2} . The resist was developed by immersion in a 1:4 solution of AZ400K developer and water for 5 min. The copper was then patterned in a PCB etch crystal solution (sodium peroxidsulfate) at 45 °C for 8 min followed by rinsing in deionized water and cleaning with acetone to strip the remaining resist.

Cutting the Filament: An Epilog Mini 24 laser cutter with a 60 W CO_2 laser with a cutting pattern resolution of 1200 dpi, repeatability of ± 0.0127 mm, and an accuracy of ± 0.0254 mm over the length of the table (600 mm) was evaluated. The laser was used to cut the Kapton after the copper surrounding the circuit was etched away. Graphtec CE600-40 with a 100 μm steel tip cutting blade was used. The cutter

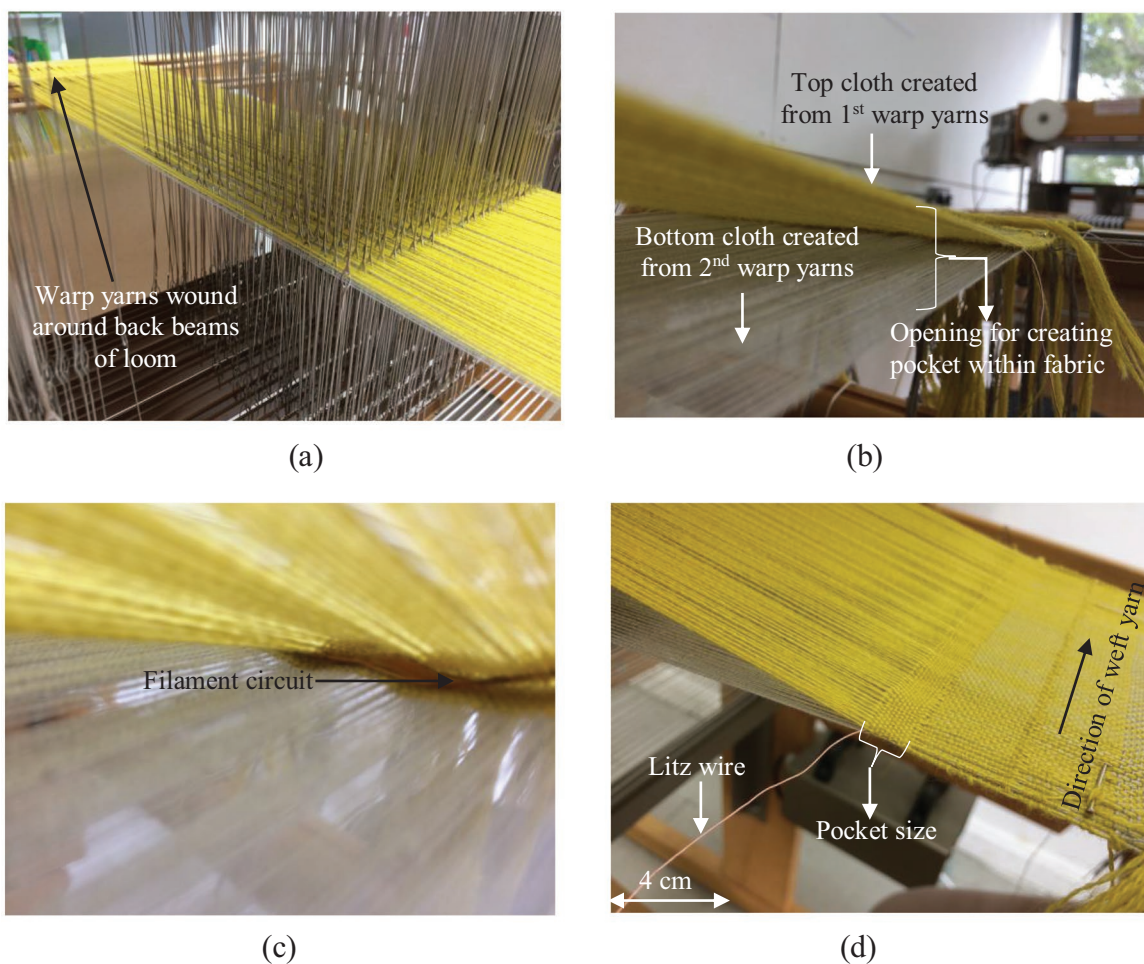


Figure 17. Weaving of filaments into fabric. (a) Loom set up for weaving a fabric swatch, b) weaving of pocket into fabric swatch, c) filament placement in pocket, and d) routing of wire in and out of the pocket.

moved at speeds up to 600 mm s^{-1} with a resolution of $10 \text{ }\mu\text{m}$ and repeatability of $100 \text{ }\mu\text{m}$.

Attachment of Components with Anisotropic Conductive Pastes: An arbitrary volume of anisotropic conductive paste (Elecolit 3061 from Eurobond Adhesives Ltd.) was manually dispensed on to a flat alumina plate as shown in Figure 5a. The component was picked up and dipped into the ACP using the pick and place tool such that the adhesive formed a glob on the bottom of the component. The filament substrate was positioned on the heating plate of the Finetech tool and the component was aligned and positioned with a bonding force of 10 N (contact pressure of 130 MPa) and heated up to $100 \text{ }^\circ\text{C}$ in 10 s, held for 60 s, and then cooled.

Attachment of Components with Solder Paste: Solder paste was printed using a $100 \text{ }\mu\text{m}$ thick stainless steel stencil aligned with the substrate producing solder bumps on the surface as shown in Figure 5b. The filament was positioned on the heating plate and the component aligned and then lowered onto the substrate. The bond was formed using the temperature profile in Table 3. To improve the mechanical attachment of the chip to the substrate, Loctite 4902 was used as underfill. This was dispensed just after stencil printing the solder paste and was heated simultaneously with the solder paste to bond the chip to the filament. Components supplied with solder bumps were initially dipped into a small volume of solder-flux paste to aid the flow and wetting of the solder on the copper bond pads. The component was then aligned on the filament and bonded using the temperature profile in Table 3.

Weaving Filament Circuits into Fabric: A Toika dobby weaving loom was used to integrate the filaments into the fabric. The filament circuits were positioned in narrow pockets that were created as part of the fabric weaving process. The bespoke pockets were formed within the fabric using a double cloth (or double weave) setup. This involved weaving two or more sets of warp and one or more set of weft yarns that formed two layers of fabric interlaced together by one of the weft yarns.^[54] Two sets of warp yarns were wound on two separate wooden back beams of the loom and guided through metallic heddles as shown in Figure 17a. These series of warps were woven with individual weft or filling yarns to make two layers of cloth with a plain weave structure for making a strong, stable, and even fabric.^[54] The pocket was created when the position of the top cloth and the bottom cloth was interchanged, i.e., the top cloth became the bottom cloth and vice versa. This created a stitched line across the fabric, a woven intersection of both fabric layers that opened up the pocket as shown in Figure 17b and repeating the process at the required point in the weave design closed the pocket. The filament was manually inserted immediately the pocket was created (Figure 17c) and the connecting copper wires from the filaments were manually routed at the same time as shown in Figure 17d. The optimum wire for this process was found to be a silk coated multistrand Litz wire that moved feely within the woven pockets. This weaving method can create vertical and horizontal pockets within the fabric for routing the wires and the filaments in the warp and weft directions as required.

Bending Test: The bending rig, shown in Figure 9a, was used to cyclically strain the LED filament circuits. The bending rig was driven by a stepper motor that moved the sample holder backward and forward with the test sample being folded around a specified radius. The 1.5 N tension in the sample was defined by the weight of the sample holder and plate attached to the other end of the sample. The LED filaments were powered during the test and cycled around bending radii of 1.5, 5, and 10 mm until the LED blinked or failed completely. A total of 171 LED filament circuits were tested of which 54 were integrated into the fabric swatch as shown in Figure 7c.

Washing Test: The swatches containing the filament circuits were loaded with seven other clothes in a domestic washing machine for five washing cycles that consisted of a 58 min wash at a temperature of $40 \text{ }^\circ\text{C}$ with a 1000 rpm spin dry cycle. The fabrics were washed in a commercial Beko washing machine WME7247W with the DAZ washing detergent for every wash cycle. This wash cycle was chosen to closely replicate the normal washing procedure as stated in the ISO 6330:2000-6A washing standard.^[53] To enhance the durability of the filaments, the Litz wires extending from the power supply bond pads

of the filaments were stitched to the swatches before washing using a PFAFF Creative 3.0 sewing and embroidery machine. The samples were washed without the battery.

Acknowledgements

The authors thank EPSRC for supporting this research with grant reference EP/M015149/1.^[55]

Conflict of Interest

The authors declare no conflict of interest.

Keywords

durable e-textiles, wearable e-textiles, woven filament circuits

Received: February 26, 2019

Revised: May 9, 2019

Published online: June 13, 2019

- [1] F. Axisa, P. M. Schmitt, C. Gehin, G. Delhomme, E. McAdams, A. Dittmar, *IEEE Trans. Inf. Technol. Biomed.* **2005**, *9*, 325.
- [2] L. M. Castano, A. B. Flatau, *Smart Mater. Struct.* **2014**, *23*, 053001.
- [3] K. Cherenack, L. van Pieterse, *J. Appl. Phys.* **2012**, *112*, 091301.
- [4] K. J. Heilman, S. W. Porges, *Biol. Psychol.* **2007**, *75*, 300.
- [5] R. Ma, J. Lee, D. Choi, H. Moon, S. Baik, *Nano Lett.* **2014**, *14*, 1944.
- [6] T. Hughes-Riley, P. Lugoda, T. Dias, C. L. Trabi, R. H. Morris, *Sensors* **2017**, *17*, 1804.
- [7] R. Bhattacharya, L. van Pieterse, K. van Os, *IEEE Trans. CPMT* **2012**, *2*, 165.
- [8] N. Taccini, G. Loriga, A. Dittmar, R. Paradiso, presented at *Proc. of the 26th Annual Int. Conf. of the IEEE EMBS*, San Francisco, CA, September **2004**.
- [9] N. Noury, A. Dittmar, C. Corroy, R. Baghai, J. L. Weber, D. Blanc, F. Klefsat, A. Blinowska, S. Vaysse, B. Cornet, presented at *26th Annual Int. Conf. of the IEEE Engineering in Medicine and Biology Society*, San Francisco, CA, September **2004**.
- [10] I. Locher, M. Klemm, T. Kirstein, G. Trster, *IEEE Trans. Adv. Packag.* **2006**, *29*, 777.
- [11] D. Patron, W. Mongan, T. P. Kurzweg, A. Fontecchio, G. Dion, E. K. Anday, K. R. Dandekar, *IEEE Trans. Biomed. Circuits Syst.* **2016**, *10*, 1047.
- [12] D. Curone, E. L. Secco, A. Tognetti, G. Loriga, G. Dudnik, M. Risatti, G. Magenes, *IEEE Trans. Inf. Technol. Biomed.* **2010**, *14*, 694.
- [13] M. A. Oleson, C. Dibenedetto, S. Tomlinson, A. W. Van Noy, A. J. Vaterlaus, S. M. Vincent, *U.S. Patent 9,645,165*, **2017**.
- [14] N. Davies, *AATCC Rev.* **2017**, *17*, 46.
- [15] E. R. Post, M. Orth, P. R. Russo, N. Gershenfeld, *IBM Syst. J.* **2000**, *39*, 840.
- [16] X. Tao, V. Koncar, T. H. Huang, C. L. Shen, Y. C. Ko, G. T. Jou, *Sensors* **2017**, *17*, 673.
- [17] S. de Mulatier, M. Nasreldin, R. Delattre, M. Ramuz, T. Djenizian, *Adv. Mater. Technol.* **2018**, *3*, 1700320.
- [18] J. S. Heo, T. Kim, S. G. Ban, D. Kim, J. H. Lee, J. S. Jur, S. K. Park, *Adv. Mater.* **2017**, *29*, 1701822.
- [19] Y. Kim, H. Kim, H. Yoo, *IEEE Trans. Adv. Packag.* **2010**, *33*, 857.
- [20] M. A. Yokus, R. Foote, J. S. Jur, *IEEE Sens. J.* **2016**, *16*, 7967.

- [21] W. Dang, V. Vinciguerra, L. Lorenzelli, R. Dahiya, *Flexible Printed Electron.* **2017**, 2, 013003.
- [22] J. Byun, E. Oh, B. Lee, S. Kim, S. Lee, Y. Hong, *Adv. Funct. Mater.* **2017**, 27, 1701912.
- [23] J. Yoon, Y. Jeong, H. Kim, S. Yoo, H. S. Jung, Y. Kim, S. H. Choa, *Nat. Commun.* **2016**, 7, 11477.
- [24] K. Yang, R. Torah, Y. Wei, S. Beeby, J. Tudor, *Text. Res. J.* **2013**, 83, 2023.
- [25] A. Komolafe, R. Torah, J. Tudor, S. Beeby, *Proceedings* **2017**, 1, 613.
- [26] A. Almusallam, Z. Luo, A. Komolafe, K. Yang, A. Robinson, R. Torah, S. Beeby, *Nano Energy* **2017**, 33, 146.
- [27] M. De Vos, R. Torah, M. Glanc-Gostkiewicz, J. Tudor, *J. Disp. Technol.* **2016**, 12, 1757.
- [28] C. R. Merritt, H. T. Nagle, E. Grant, *IEEE Trans. Inf. Technol. Biomed.* **2009**, 13, 274.
- [29] K. Yang, C. Freeman, R. Torah, S. Beeby, J. Tudor, *Sens. Actuators, A* **2014**, 213, 108.
- [30] A. O. Komolafe, R. N. Torah, M. J. Tudor, S. P. Beeby, *Smart Mater. Struct.* **2018**, 27, 075046.
- [31] G. A. Salvatore, N. Münzenrieder, C. Zysset, T. Kinkeldei, L. Petti, G. Tröster, presented at *IEEE 36th Annual EMBC Int. Conf.*, Chicago, IL, August **2014**.
- [32] C. Zysset, T. W. Kinkeldei, N. Munzenrieder, K. Cherenack, G. Troster, *IEEE Trans. Compon., Packag., Manuf. Technol.* **2012**, 2, 1107.
- [33] K. H. Cherenack, T. Kinkeldei, C. Zysset, G. Troster, *IEEE Electron Device Lett.* **2010**, 31, 740.
- [34] S. Takamatsu, T. Yamashita, T. Itoh, in *IEEE Symp. on DTIP of MEMS and MOEMS*, Montpellier, April **2015**.
- [35] J. Fjelstad, *Flexible Circuit Technology*, 3rd ed., BR Publishing, Incorporated, Seaside, OR, USA **2018**.
- [36] C. Zysset, T. Kinkeldei, N. Münzenrieder, L. Petti, G. Salvatore, G. Tröster, *Text. Res. J.* **2013**, 83, 1130.
- [37] K. Cherenack, C. Zysset, T. Kinkeldei, N. Münzenrieder, G. Tröster, *Adv. Mater.* **2010**, 22, 5178.
- [38] D. Hardy, I. Anastasopoulos, M. N. Nashed, C. Oliveira, T. Hughes-Riley, A. Komolafe, T. Dias, presented at *IEEE Symp. on DTIP*, Roma, Italy, May **2018**.
- [39] C. Müller, M. Hamedi, R. Karlsson, R. Jansson, R. Marcilla, M. Hedhammar, O. Inganäs, *Adv. Mater.* **2011**, 23, 898.
- [40] M. Hamedi, R. Forchheimer, O. Inganäs, *Nat. Mater.* **2007**, 6, 357.
- [41] D. H. Kim, Y. S. Kim, J. Wu, Z. Liu, J. Song, H. S. Kim, J. A. Rogers, *Adv. Mater.* **2009**, 21, 3703.
- [42] A. R. Köhler, L. M. Hilty, C. Bakker, *J. Ind. Ecol.* **2011**, 15, 496.
- [43] A. R. Köhler, *Mater. Des.* **2013**, 51, 51.
- [44] M. Li, J. Tudor, R. Torah, S. Beeby, presented at *67th IEEE Electronic Components and Technology Conf. (ECTC)*, Florida, USA, May **2017**.
- [45] M. Li, J. Tudor, R. Torah, S. Beeby, *IEEE Trans. Compon., Packag., Manuf. Technol.* **2018**, 8, 186.
- [46] H. Ushijima, Y. Kusaka, M. Fujita, K. I. Nomura, S. Kanazawa, Y. Horii, N. Yamamoto, presented at *Int. Conf. on Electronics Packaging (ICEP)*, Yamagata, Japan, April **2017**.
- [47] P. S. Chauhan, A. Choubey, Z. Zhong, M. G. Pecht, *Copper Wire Bonding*, Springer, New York **2014**.
- [48] GTS Flexible Materials Ltd., GTS 7800 - Copper polyimide laminates, GTS Ultraflex datasheet, <http://pwcircuits.co.uk/pwcircuits/wp-content/uploads/2018/08/GTS78001.pdf> (accessed: May 2019).
- [49] PCB Trace Width Calculator, <http://circuitcalculator.com/wordpress/2006/01/31/pcb-trace-width-calculator/> (accessed: May 2019).
- [50] W. Engelmaier, A. Wagner, *Circuit World* **1988**, 14, 30.
- [51] J. Zhu, J. Feng, Z. Guo, *RSC Adv.* **2014**, 4, 57671.
- [52] M. Li, J. Tudor, J. Liu, R. Torah, A. Komolafe, S. Beeby, *IEEE Trans. CPMT* **2019**, 9, 216.
- [53] A. Komolafe, *Ph.D. Thesis*, University of Southampton **2016**.
- [54] N. Gokarneshan, *Fabric Structure and Design*, New Age International Ltd., New Delhi, India **2004**.
- [55] Novel manufacturing methods for functional electronic textiles <http://gow.epsrc.ac.uk/NGBOViewGrant.aspx?GrantRef=EP/M015149/1> (accessed: May 2019).